

Coherent nonlinear optics with quantum cascade structures

ALEXEY BELYANIN*[†], FENG XIE[†], DEBIN LIU[†],
FEDERICO CAPASSO[‡] and MARIANO TROCCOLI[‡]

[†]Department of Physics, Texas A&M University,
College Station, Texas 77843, USA

[‡]Division of Engineering and Applied Sciences,
Harvard University, Cambridge, Massachusetts 02138, USA

(Received 15 February 2005; in final form 7 April 2005)

We discuss several coherent nonlinear optical phenomena that occur in active quantum-cascade (QC) structures that support both laser action and, at the same time, nonlinear self-conversion of laser light into coherent radiation at other frequencies. In other words, the laser field serves as an intracavity optical pump for a desired nonlinear optical process. In such systems, resonant absorption of the pump field is overcome by laser gain, and giant resonant nonlinearities of the intersubband transitions can be fully exploited. The proposed approach holds promise to extend the operating wavelength of QC lasers to the spectral regions where they become less efficient, constrained by material limitations, or operate only at cryogenic temperatures. It may also lead to the development of new broadly tunable injection-pumped sources. We review recent development in this research direction including the demonstration of the Raman injection laser.

1. Introduction

It has been demonstrated since the 1980s that a system of n-doped coupled quantum wells can exhibit very large resonant optical nonlinearities associated with inter-subband transitions [1–5]. For example, experiments with second-harmonics and difference-frequency generation in $\text{In}_x\text{Ga}_{1-x}\text{As}/\text{Al}_{1-y}\text{In}_y\text{As}$ and $\text{GaAs}/\text{Al}_x\text{Ga}_{1-x}\text{As}$ quantum wells using a CO_2 laser as an external pump demonstrated the second-order nonlinear susceptibility $\chi^{(2)}$ of the order of 10^{-7} m V^{-1} in the mid-infrared range and 10^{-6} m V^{-1} in the far infrared. This is to be compared with a few picometres per volt in standard nonlinear optical materials such as potassium dihydrogen phosphate or lithium niobate, and with hundreds of picometres per volt in bulk GaAs or InP. Such giant nonlinear susceptibilities originate from several factors.

*Corresponding author. Email: belyanin@tamu.edu

Firstly, there is the n th-order resonance in the n th-order nonlinear susceptibility, which leads to a sharp enhancement of its magnitude.

The second factor enabling large nonlinearities is the huge dipole moments of the intersubband transitions that can be of the order of 2–3 nm in the mid-infrared range and several times higher in the far infrared. Even more important is the possibility of manipulating oscillator strengths in the coupled quantum wells and basically making all transitions allowed. Note that in atoms the situation when all three transitions between states 1, 2 and 3, shown later in figure 1, are dipole allowed is virtually impossible.

Unfortunately, despite this great potential of the intersubband transitions for nonlinear optics, the nonlinear power measured in this kind of experiments was at the nanowatt level at best, even with a high-power CO₂ laser pump. The reason for such a low efficiency and power was a very small interaction length, limited to a few micrometres in the multipass geometry. In fact, this problem cannot be solved

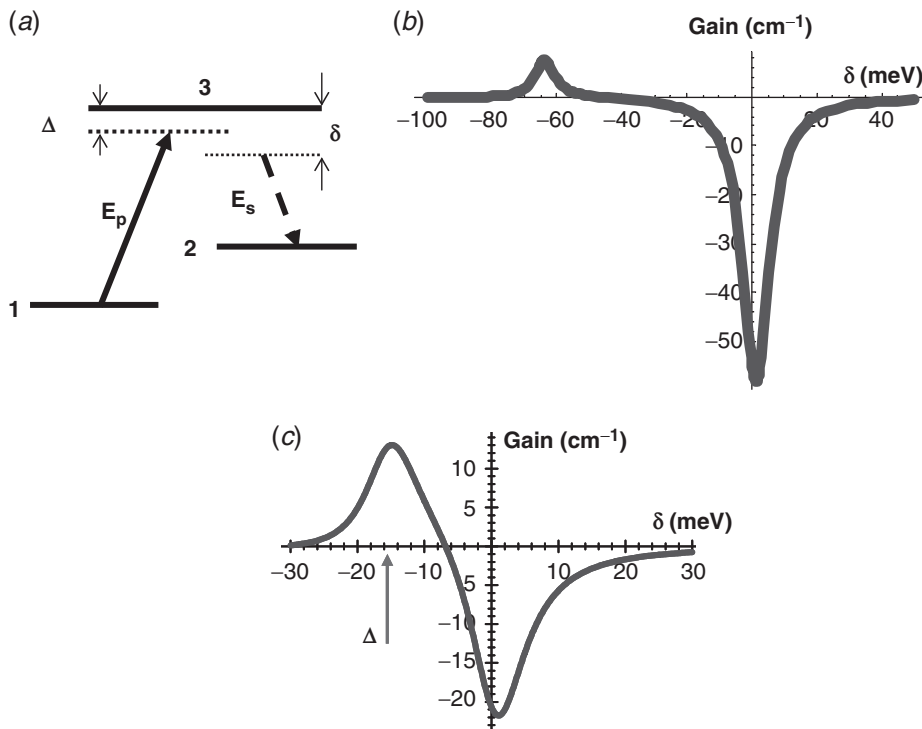


Figure 1. (a) A schematic diagram of the Raman scattering of laser light (solid arrow) into a lower-frequency Stokes wave (dashed arrow). (b) Calculated Raman gain spectrum when the detuning Δ is much larger than linewidth. (c) Stokes gain spectrum calculated using equation (1) for the structure shown in figure 2, with the detuning Δ equal to 15 meV. The arrow indicates the position of the two-photon resonance $\omega_p - \omega_s = \omega_{21}$.

by choosing a more favourable geometry for the experiment. There is fundamental limitation on the nonlinear efficiency stemming from the following problems.

- (i) *Strong resonant absorption that limits the interaction length and conversion efficiency.* With tuning to resonance, nonlinear susceptibilities are becoming larger but so is the resonant absorption. The linear absorption in intersubband transitions becomes of the order of 1000 cm^{-1} for the doping level of a few 10^{11} cm^{-2} . As a result, one is left with two choices: either to decrease the propagation length or to reduce the overlap of the electromagnetic modes with the absorbing nonlinear medium. In both cases the nonlinear efficiency will be low for all practical devices. This is actually a fundamental limitation that forces nonlinear optical devices to operate in the transparency region, far away from any resonances.
- (ii) *Phase matching.* The mismatch of the wave vectors of the interacting modes in the mid-infrared range is of the order of 1000 cm^{-1} . Standard techniques of angle and quasiphase matching are difficult to implement owing to the lack of birefringence and ferroelectricity in III–V semiconductors. An alternative, very elegant approach is to exploit waveguide modes of different types and orders, so that the waveguide dispersion compensates for the material dispersion. This idea can be traced back to [6] and has been recently exploited for a variety of nonlinear processes and materials [7–9]. However, coupling of an external laser beam incident on a facet of a structure to a given transverse mode of a semiconductor waveguide is difficult to realize, and absorption and scattering losses limit the conversion efficiency.
- (iii) Coupling of an external optical pump with the nonlinear medium is inefficient owing to a variety of problems related to polarization selection rules, reflection and scattering losses of the pump, inhomogeneity of the field distribution in the sample, etc.

The combination of the above fundamental and technical challenges seems to make intersubband transitions impractical for most applications in nonlinear optics. The way to overcome these challenges and to exploit fully the benefits of resonant nonlinear optics has been identified theoretically [10, 11] and confirmed recently in a series of experiments with nonlinear generation in quantum-cascade (QC) lasers [12–18].

The main idea is to integrate monolithically an active laser medium and the nonlinear medium in such a way that the laser field could serve as an intracavity optical pump for the desired nonlinear optical interaction. Basically, we are dealing with *active* nonlinear systems that support both laser action and, at the same time, nonlinear self-conversion of laser light into the coherent radiation at other frequencies. With application to intersubband transitions, this means that we want to incorporate the nonlinear section (usually a coupled quantum well containing a cascade of intersubband transitions) directly into the active region of a QC laser.

Clearly, QC structures are ideal candidates for this integration because of their unique efficiency in controlling the electron transport, lifetimes and populations of

electron states in combination with flexibility of the active region design. It is also important that there is no cross-absorption between intersubband transitions at different frequencies because different subbands have similar dispersions (their effective masses are very similar and non-parabolicity is usually small).

2. Resonant Raman laser

In a general scheme of the stimulated Raman scattering sketched in figure 1, the incident photon of energy $\hbar\omega_p$ is converted into a Stokes photon of energy $\hbar\omega_s$. The underlying physical mechanism is scattering of the incident fundamental radiation by a certain eigenmode of oscillations in a material, which is self-consistently excited by the parametric interaction between the incident and the scattered light. The wavelength shift between the fundamental emission and the Raman emission is determined by the resonance frequency of the internal oscillations and can be due to vibrational (phonon), rotational, plasmon or electronic resonances.

Stimulated Raman scattering has been observed in all kinds of medium: gases, liquids, solids and plasmas. Until now, a distinctive feature of all Raman amplifiers has been the necessity for an external optical pump. Also, existing solid-state Raman sources universally employ scattering off a vibrational (phonon) resonance in a crystal or fibre [19]. A powerful fundamental laser radiation is usually required to offset a small value of the Raman gain (several 10^{-9} cm W $^{-1}$).

The possibility of Raman amplification using intersubband transitions has been theoretically discussed in [20]. In recent work [21], Raman lasing on intersubband transitions in a GaAs/Al $_x$ Ga $_{1-x}$ As double-quantum-well structure optically pumped by a CO $_2$ laser has been demonstrated, although the Raman shift was still determined by a phonon resonance. In recent work [17] we demonstrated the first *injection-pumped* Raman laser, where the fundamental and the Raman radiations are both generated by intersubband electronic transitions in the very same active region of a QC laser. The stimulated scattering and lasing are due to the excitation of coherent electronic polarization on the mid-infrared intersubband transition 2–1. Its frequency $(E_2 - E_1)/\hbar$ defines the Raman shift; it has nothing to do with phonons and can vary in a very broad range. It could be also efficiently tuned by a voltage bias since the transition 2–1 is diagonal in real space.

One period of the Raman laser structure reported in [17] is shown in figure 2(a). Laser light at 6.7 μ m generated in the transition 6–5 serves as a resonant optical pump for lasing at the Stokes wavelength of 9 μ m, which is detuned by 15 meV from the transition 3–2. Resonant absorption of the pump at the transition 1–3 is overcome by amplification in the pump laser section at the transition 6–5. The triply resonant nature of the process makes Raman scattering very efficient; the peak fundamental power is only 40 mW at the threshold for Raman lasing (figure 2(b)), which implies a very large gain coefficient of the order of 2×10^{-5} cm W $^{-1}$ per period (6×10^{-4} cm W $^{-1}$ for the whole stack of 30 stages) and high efficiency of the nonlinear interaction. The nonlinear conversion efficiency around 30% has been measured.

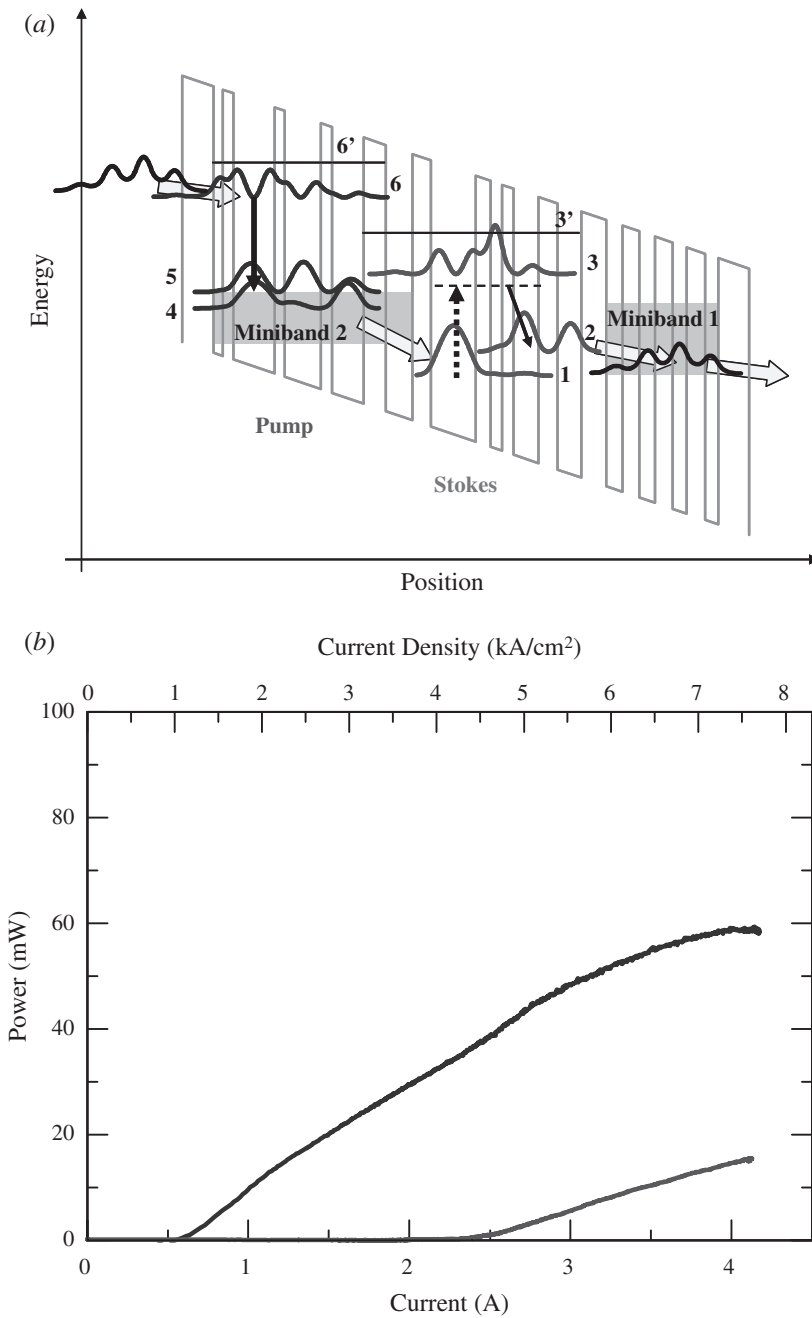


Figure 2. (a) Active region of a resonant Raman laser that integrates the fundamental laser cascade 6–5–4 and resonant Λ scheme of transitions 1–3–2–1 for Raman Stokes lasing. (b) Laser (upper curve) and Stokes (lower curve) powers as functions of the injection current.

The modal gain at the Stokes frequency can be found from solving the coupled density-matrix equations and Maxwell's equations for transverse magnetically polarized laser modes. We assume for simplicity that all intersubband transitions are homogeneously broadened and have the Lorentzian line shape. This is supported by numerous absorption and electroluminescence measurements in QC structures. The broadening is mainly due to interface roughness [22]. However, this assumption can be easily dropped if one needs to include non-parabolicity and other effects leading to inhomogeneous broadening. We also neglect many-body effects originating from Coulomb interaction of electrons. For the low 10^{11} cm^{-2} doping levels relevant to QC laser structures, Coulomb interaction leads to a line shift of the order of 1 meV, which is much less than the total linewidth. The resulting expression for the gain spectrum is as follows:

$$g = \frac{4\pi\omega_S e^2 z_{32}^2 \Gamma_S}{\hbar c \mu_S} \text{Re} \left[\frac{1}{\Gamma_{32} + |\Omega_p|^2 / \Gamma_{21}^*} \left(\frac{|\Omega_p|^2 (n_1 - n_3)}{\Gamma_{21}^* \Gamma_{31}^*} - (n_2 - n_3) \right) \right]. \quad (1)$$

Here $\Gamma_{32} = \gamma_{32} + i(\omega_S - \omega_{32})$, $\Gamma_{31} = \gamma_{31} + i(\omega_p - \omega_{31})$, $\Gamma_{21} = \gamma_{21} + i(\omega_p - \omega_S + \omega_{21})$, $\Omega_p = ez_{13}E_p/\hbar$ is the Rabi frequency of the optical pump, E_p is its electric field amplitude, z_{mn} is the dipole moment of the transition m - n , ω_{mn} is the transition frequency, ω_p and ω_S are the frequencies of the pump and the Stokes field respectively, Γ_S is the optical confinement factor for the Stokes mode and $\mu_S = 3.2$ is its refractive index. Typical values of dephasing rates γ_{mn} are 5 meV for $\text{In}_x\text{Ga}_{1-x}\text{As}/\text{Al}_{1-y}\text{In}_y\text{As}$ quantum wells. We obtained these from luminescence measurements. The optical pump field and population densities $n_{1,2,3}$ of electrons in states 1, 2, 3 are not free parameters. They are calculated self-consistently for a given injection current from the same set of coupled density-matrix and the Maxwell equations.

The first term in large parentheses in equation (1) is due to parametric beating between the pump field and the off-diagonal density matrix element ρ_{12} (Raman coherence), where the latter is excited self-consistently by beating between the pump and the signal fields. The second term, proportional to $n_2 - n_3$, is due to linear absorption of a signal in the transition 2–3. Under our conditions the first term is much larger than the second term. The gain, evaluated at the threshold for the Stokes lasing using equation (1), is shown in figure 1(c). In the limit of very large detuning Δ , shown in figure 1(b), the gain in equation (1) is reduced to

$$g = \frac{4\pi\omega_S e^4 z_{32}^2 \Gamma_S |\Omega_p|^2 (n_1 - n_2)}{\hbar c \mu_S \Delta^2 \gamma_{21}},$$

that is it becomes proportional to the Raman inversion $n_1 - n_2$ and inversely proportional to the relaxation rate γ_{21} of the Raman coherence. In this case, real one-photon transitions to the excited state 3 with subsequent emission of a photon due to de-excitation to state 2 are much less probable than the two-photon transitions from state 1 to state 2 through an intermediate state. Note that this limit is not identical with just dropping the linear absorption term from equation (1).

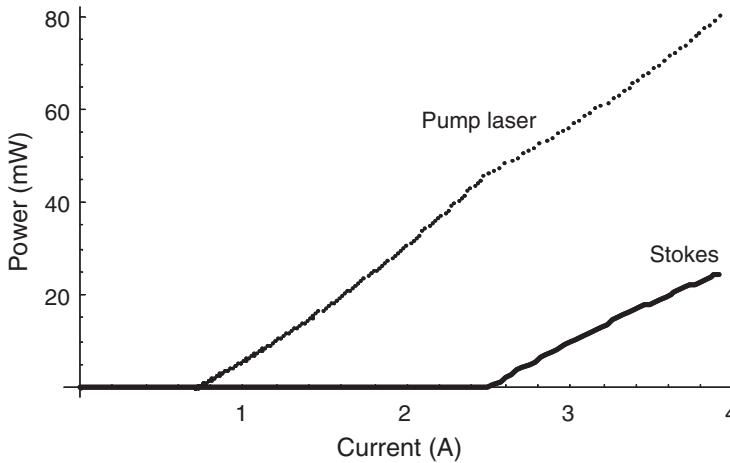


Figure 3. The calculated power of the pump laser and the Stokes field as functions of the injection current for the devices reported in [17].

An example of theoretical modelling of the nonlinear dynamics of laser and Stokes modes is shown in figure 3. Apparently, the modelling accurately predicts both thresholds but yields larger values for the Stokes slope efficiency and does not show any signs of the rollover of the laser pump at 60 mW, contrary to what is observed in figure 2(b). Most probably, the fundamental laser deteriorated owing to misalignment in the resonant electron tunnelling through the cascade. This is a common problem with QC lasers far above threshold. It can be circumvented by designing a broader injector miniband. The Stokes laser power rolls off simultaneously with the roll-off of the pump laser. However, data in this region are not reliable; so they are not shown in figure 2(b).

An interesting feature of the nonlinear dynamics in our integrated devices is that there is gain for both the fundamental laser pump and the Stokes signal. Thus, both waves are simultaneously amplified. In particular, gain compensates for both linear absorption and nonlinear depletion of the pump. Therefore, such Raman lasers beat Manley–Rowe relations that require one pump photon to be absorbed for each Stokes photon created. This could potentially lead to much higher efficiencies of frequency downconversion compared with conventional Raman lasers and other nonlinear optical devices. The energy is, of course, drawn from the injection current.

3. Lasing without inversion

The physics of resonant Raman lasing are similar to those of lasing without inversion (LWI)—a quantum-optical phenomenon that has been the subject of much debate since its theoretical prediction 15 years ago [23–25]. Until now, LWI has been realized only in proof-of-principle experiments in rarified atomic

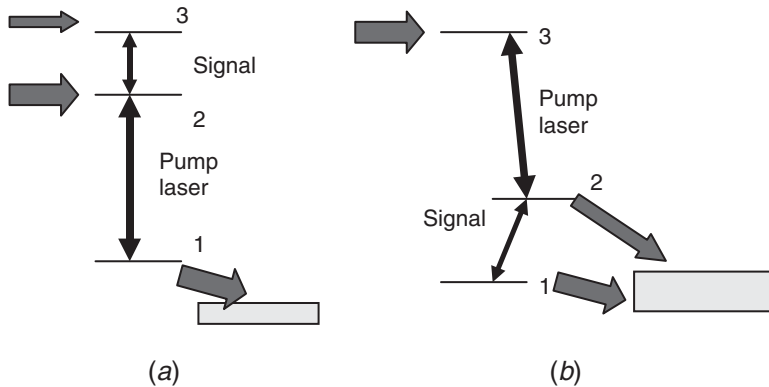


Figure 4. Lasing without inversion in (a) the lower-ladder scheme and (b) the upper-ladder scheme. The pump laser transition coincides with one leg of the inversionless cascade. Shaded rectangles indicate injector states in minibands. Arrows indicate injection current.

vapours (see [26] for a review). In principle, to obtain inversionless lasing in the Λ scheme of figure 1(a), one does not need any kind of inversion including Raman inversion, although we did have Raman inversion $n_1 - n_2 > 0$ under our experimental conditions. Moreover, modelling shows that in most cases of practical interest there is Raman-type inversion between the initial and final states of the two-photon transition in any three-level scheme (e.g. $n_3 > n_1$ in figure 4(b)). Therefore, the term LWI should be treated with caution.

In the above Λ -type Raman schemes the optical pump field and the inversionless signal are generated in adjacent but physically different coupled-quantum-well active regions. In this approach, pump laser and LWI active regions are optimized separately, adding flexibility to the design; yet they necessarily compete for the overlap with optical modes in the waveguide. In the second approach that we describe below, both the optical pump and the signal are generated in the same coupled-quantum-well active region, so that the pump laser transition serves as one leg of the LWI cascade. This approach has the advantage of using as much of the waveguide core as possible for both the pump laser gain and the LWI process, although trade-off may exist between the pump laser performance and the LWI gain. Our theoretical analysis yields two schemes that provide maximum LWI gain: the upper- and lower-ladder schemes given in figures 4(a) and (b) respectively.

In the lower-ladder scheme in figure 4(a), the optical pump field is generated in the transition 2–1. There is population inversion between states 2 and 1 owing to the very fast depletion of state 1 and relatively long lifetime of state 2. The laser field generated in the transition 2–1 serves as a coherent drive for the inversionless lasing in a rapidly decaying lower-frequency transition 3–2. Block arrows show the injection current of electrons. In the upper laser scheme in figure 4(b) the roles of transitions 1–2 and 2–3 are interchanged. Now the transition 3–2 is inverted and supports pump laser generation, while the signal is generated in the transition 1–2 in the absence of population inversion in this transition.

In both schemes the maximum gain is achieved exactly at resonance $\omega_{\max} = \omega_{32}$ or $\omega_{\max} = \omega_{21}$ respectively. The pump field is automatically at resonance with a corresponding laser transition. Its wavelength should be chosen in the optimum performance range for QC lasers: between 7 and 9 μm . Both frequency upconversion and downconversion are possible in both schemes. Detailed analysis can be found in [11].

The gain in all three-level LWI schemes has a structure very similar to that in equation (1). For example, for the scheme in figure 4(b) the peak gain is given by

$$g = \frac{4\pi\omega_S e^2 z_{21}^2}{\hbar c \mu_S (\gamma_{21} + |\Omega_p|^2 / \gamma_{31})} \left(\frac{|\Omega_p|^2 (n_3 - n_2)}{\gamma_{32} \gamma_{31}} - (n_1 - n_2) \right). \quad (2)$$

The gain is due to the competition between the ‘coherence’ term, proportional to the pump field intensity and population difference in the optical pumping transition, and the linear absorption of a signal, proportional to the population difference in the signal transition.

There are many other kinds of monolithically integrated nonlinear QC laser sources that we are not able to discuss because of space limitations. They include anti-Stokes Raman laser, parametric downconversion and oscillation, and sum-frequency and difference-frequency generation in two-wavelength QC lasers. An attractive feature of all these novel devices is that they promise to combine the flexibility and tunability of nonlinear optical devices with robustness, ultra-compact size, low power consumption, and convenience of semiconductor injection lasers. Also, there are interesting prospects to cover the spectral regions where QC lasers become less efficient, constrained by material limitations, or operate only at cryogenic temperatures. Possible examples include nonlinear frequency upconversion to the 3–5 μm range via generation of harmonics, anti-Stokes Raman scattering, or LWI, and nonlinear frequency downconversion to the terahertz range via Stokes Raman lasing.

Acknowledgments

This work was supported in part by the National Science Foundation and the Air Force Office of Scientific Research.

References

- [1] M.K. Gurnick and T.A. De Temple, *IEEE J. Quant. Electron* **19** 791 (1983).
- [2] M.M. Fejer, S.J.B. Yoo, R.L. Byer, *et al.*, *Phys. Rev. Lett.* **62** 1041 (1989).
- [3] C. Sirtori, F. Capasso, D.L. Sivco, *et al.*, *Appl. Phys. Lett.* **59** 2302 (1991).
- [4] F. Capasso, C. Sirtori, D.L. Sivco, *et al.*, *Physics and Device Applications II* (Academic Press, San Diego, CA, 2000).
- [5] J.B. Khurgin, E. Garmire and A. Kost, in *Nonlinear Optics in Semiconductors II* (Academic Press, San Diego, CA, 1999).
- [6] J.P. Van der Ziel, *Appl. Phys. Lett.* **26** 60 (1975).
- [7] A. Fiore, V. Berger, E. Rosencher, P. Bravetti and J. Nagle, *Nature* **391** 463 (1998).

- [8] A. Chowdhury and L. McCaughan, *IEEE Photonics Technol. Lett.* **12** 486 (2000).
- [9] K. Moutzouris, S.V. Rao, *et al.*, *Appl. Phys. Lett.* **83** 620 (2003).
- [10] A.A. Belyanin, F. Capasso, V.V. Kocharovsky, *et al.*, *Phys. Rev. A* **63** 053 803 (2001).
- [11] A.A. Belyanin, C. Bentley, F. Capasso, *et al.*, *Phys. Rev. A* **64** 013 814 (2001).
- [12] N. Owschimikow, C. Gmachl, A. Belyanin, *et al.*, *Phys. Rev. Lett.* **90** 043 902 (2003).
- [13] C. Gmachl, A. Belyanin, D.L. Sivco, *et al.*, *IEEE J. Quant. Electron.* **39** 1345 (2003).
- [14] O. Malis, A. Belyanin, C. Gmachl, *et al.*, *Appl. Phys. Lett.* **84** 2721 (2004).
- [15] C. Gmachl, N. Owschimikow, A. Belyanin, *et al.*, *Appl. Phys. Lett.* **84** 2751 (2004).
- [16] T.S. Mosely, A. Belyanin, C. Gmachl, *et al.*, *Optics Express* **12** 2972 (2004).
- [17] M. Troccoli, A. Belyanin, F. Capasso, *et al.*, *Nature* **433** 845 (2005).
- [18] O. Malis, A. Belyanin, D.L. Sivco, *et al.*, *Electron. Lett.* **40** 1586 (2004).
- [19] H.M. Pask, *Prog. Quant. Electron.* **27** 3 (2003).
- [20] G. Sun, J. Khurgin, L. Friedman, *et al.*, *J. Opt. Soc. Am. B* **15** 648 (1998).
- [21] H.C. Liu, Iva W. Cheung, A.J. SpringThorpe, *et al.*, *Appl. Phys. Lett.* **78** 3580 (2001).
- [22] J. Faist, C. Sirtori, F. Capasso, *et al.*, *Appl. Phys. Lett.* **64** 872 (1994).
- [23] O. Kocharovskaya and Ya.I. Khanin, *JETP Lett.* **48** 581 (1988).
- [24] S.E. Harris, *Phys. Rev. Lett.* **62** 1033 (1989).
- [25] M.O. Scully, S.Y. Zhu and A. Gavrielides, *Phys. Rev. Lett.* **62** 2813 (1989).
- [26] J. Mompert and R. Corbalán, *Quant. Semiclass. Optics* **2** R7 (2000).

Copyright of Journal of Modern Optics is the property of Taylor & Francis Ltd. The copyright in an individual article may be maintained by the author in certain cases. Content may not be copied or emailed to multiple sites or posted to a listserv without the copyright holder's express written permission. However, users may print, download, or email articles for individual use.